Biochimica et Biophysica Acta, 645 (1981) 33–40
Elsevier/North-Holland Biomedical Press

BBA 79292

STRUCTURE OF THE OUTER MITOCHONDRIAL MEMBRANE

ANALYSIS OF X-RAY DIFFRACTION FROM THE PLANT MEMBRANE *

CARMEN A. MANNELLA

Division of Laboratories and Research, New York State Department of Health, Albany, NY 12201 (U.S.A.)

(Received February 17th, 1981)

Key words: Membrane structure; Mitochondrial membrane; X-ray diffraction; (Plant)

X-ray diffraction from centrifugally oriented specimens of plant outer mitochondrial membranes suggests that these membranes contain prominent in-plane subunits. The short lamellar repeat which these specimens display (as low as 5.1 nm) points to a predominantly internal localization of the protein components of these membranes. The simplest model for the putative in-plane subunit consistent with autocorrelation analysis of the normal-incidence diffraction data consists of two concentric rings of electron density with diameters of (approx.) 2 and 4 nm. These rings could represent the planar projections of concentric cylindrical shells, aligned normal to the membrane surface.

Introduction

The outer membranes of isolated mitochondria are permeable to substrate-size molecules and to uncross-linked polymers as large as 5 kdaltons, but not to larger, rigid macromolecules such as holocytochrome *c* [1–4]. The electron microscopic observations of Parsons et al. [5,6] provided the first clues to the physical basis for the small-molecule permeability of this membrane. The surfaces of outer membranes of plant and mouse brain mitochondria are covered with negative-stain-filled pits, 2–3 nm in diameter, which, it was suggested, might represent aqueous pores through these membranes. In later studies on outer membranes isolated from plant mitochondria, Mannella and Bonner [7,8] identified a class of trypsin-insensitive polypeptides (M_r approx. 30 000 when electrophoresed in SDS-polyacrylamide gels) which comprise one-third to one-half of the total mass of these membranes. They also found that the X-ray diffraction from centrifugally oriented pellets of plant outer mitochondrial membranes was characterized by a series of maxima consistent with prominent subunit structure in the plane of these membranes. The diffraction maxima were unaffected by trypsinization of the membranes, implicating the 30-kdalton polypeptides as probable components of the scattering centers.

Recently, Colombini [9,10] has reported a voltage-dependent anion-specific channel-forming activity in Triton extracts of various mitochondria. This activity is concentrated in outer membrane fractions and, in the case of rat liver mitochondria, is associated with a polypeptide of M_r = 34 000 when solubilized with SDS. Subsequently, Zalman et al. [11] have reported a non-specific channel-forming activity to be associated with the prominent 30-kdalton protein(s) of plant outer mitochondrial membranes. In the case of the plant membrane, there may well be identity among the pore-forming com-

* A preliminary report of the findings of this study was presented at the 19th Annual Meeting of the American Society for Cell Biology, November, 1979, Toronto [12].

ponents, the negative-stain accumulating structures (observed in electron micrographs) and the in-plane subunits inferred from X-ray diffraction experiments. Because of this, we have undertaken a further analysis of the X-ray diffraction data from the plant outer mitochondrial membrane. In this report, we describe some simple models consistent with the observed diffraction and calculate a possible planar projection for the putative in-plane subunits of these membranes.

Results and Discussion

Multilayer structure of the membrane specimens

The procedures involved in the isolation of outer mitochondrial membranes from plant tissue (potato, *Solanum tuberosum,* and mung bean, *Phaseolus aureus*) have been described previously [4,7]. Similarly, the X-ray diffraction patterns obtained with ultracentrifugally packed specimens of these outer mitochondrial membranes, maintained at constant temperature and relative humidity under He, have already been published [8]. In the following sections X-ray diffraction spacings are given in terms of distances in reciprocal space, s, defined as $2\sin\theta/\lambda$ for X-rays of wavelength λ scattered through an angle 2θ.

The diffraction obtained with the X-ray beam at grazing incidence to the surface of an ultracentrifugally packed outer mitochondrial membrane pellet is illustrated in Fig. 1 of Ref. 8. Diffraction data along the meridian, defined as the direction in the patterns parallel to the specimen sedimentation axis, from four different membrane specimens are summarized in Table I. Three or four orders of lamellar repeat were observed in each case, indicating that the membranes had oriented into parallel multilayers during ultracentrifugation. Gradual partial dehydration of the pellets (at the relative humidities indicated in Table I) decreased the width and off-meridian spread of the lamellar arcs, indicating decreased lattice disorder in the stacking of the membranes, consistent with the loss of interplanar water. The lamellar repeat distances displayed by these specimens (as low as 5.1 nm, see Table I) approach the minimum values obtained with phospholipid-water lamellar phases (see review by Shipley [13]), suggesting that the protein components of these membranes (which make up two-thirds of the membrane mass [7]) do not extend very far from the membrane surface. This inaccessibility to the bulk aqueous phase would be consistent with the above-mentioned insensitivity of the prominent

TABLE I

MERIDIONAL X-RAY DIFFRACTION FROM PLANT OUTER MITOCHONDRIAL MEMBRANES

No.	Membrane specimen				Lamellar diffraction **		Additional maxima (nm^{-1})
	Tissue	Temp. (°C)	Relative humidity (%)	Age *	D (nm)	n_1	
1	Bean	4	75	0– 5 h	5.8	1, 2, 3, 4	1/1.1
		25	75	3– 5 days	5.5	1, 2, 3, 4	1/4.2, 1/1.1
2	Bean	10	90	1– 2 days	5.5	1, 2, 3	1/3.8, 1/1.1
3	Potato	10	75	0–24 h	5.1	1, 2, 3, 4	–
4 ***	Bean	25	75	1– 2 days	5.6	1, 2, 3	–

* Measured from the time at which membrane suspensions were pelleted.

** D = fundamental spacing or lamellar diffraction, n_1 = orders of lamellar maxima.

*** Prepared in 0.5% potassium phosphotungstate, the negative stain commonly used in electron microscopy of these membranes [6, 7, 10]. While the presence of this heavy-metal complex anion did not affect the lamellar spacing within the membrane specimen, it did result in an apparent reduction in obtainable resolution, i.e., only three orders of lamellar diffraction were detected in grazing-incidence patterns (cf. specimen 1). Similarly, only the second and third maxima of the four normally observed in normal-incidence diffraction patterns (Fig. 1 A and B) could be detected with this specimen, and a new maximum at smaller angle was also observed (see discussion in text).

30-kdalton polypeptide of these membranes to trypsin.

In addition to the lamellar reflections, additional arcs with meridional orientation were observed in the grazing-incidence X-ray diffraction patterns from several of the plant outer mitochondrial membrane specimens of Table I. The maxima near 1/4 nm^{-1} are similar to those which have been observed in X-ray diffraction patterns from other biological membranes, e.g. by Thompson et al. [14] with centrifugally packed outer and inner membranes from rat liver mitochondria. The occurrence of these nonlamellar meridional reflections is generally attributed to lateral phase separations in the membranes, which may be associated with gradual dehydration (e.g. specimen 1, Table I) or with ultracentrifugal packing [15]. The other nonlamellar meridional maxima observed in these patterns were broad arcs at 1/1.1 nm^{-1} which were only weakly oriented on the meridian. Diffuse reflections in this region are a common characteristic of biomembrane X-ray diffraction and have been attributed to protein structure, e.g. spacings between α-helices or adjacent chains in β-sheets [16–18].

Normal-incidence X-ray diffraction

Diffraction patterns obtained with X-ray beam normal to the surface of the outer mitochondrial membrane pellets display two to four rings of intensity in the region 0.3 to 1.3 nm^{-1}. Unlike the lamellar diffraction maxima discussed in the previous section, the normal-incidence diffraction rings did not vary in position (0.41, 0.67, 0.91 and 1.13 nm^{-1}, reproducible within ±0.02 nm^{-1}) with tissue, temperature (over the range 4–35°C) or age (0–5 days at 90 or 75% relative humidity). The positions of the rings in the normal-incidence diffraction patterns correspond closely to those of arcs along the equator (i.e., perpendicular to the meridian) in grazing-incidence patterns from the same or similar specimens. It was found that the strongest normal-incidence X-ray diffraction patterns (i.e., those with the best signal-to-noise ratios in microdensitometer traces) were obtained with membrane specimens after 1 or 2 days at 75 or 90% relative humidity. Fig. 1 illustrates a microdensitometer curve hand-smoothed) of the normal-incidence diffraction from specimen 1 of Table I and the background corrections applied. Curves A and B of Fig. 2 are the square-roots of the normal-incidence diffracted intensity (corrected for background and radially integrated) from both bean and potato mitochondrial outer membranes. In certain cases, smaller-angle maxima were also detected in the normal-incidence diffraction patterns, e.g. at 0.17 nm^{-1} for specimen 1 (curve A of Fig. 2) and at 0.28 nm^{-1} for specimen 4 (prepared in 0.5% potassium phosphotungstate; scattering curve not shown; see foot-

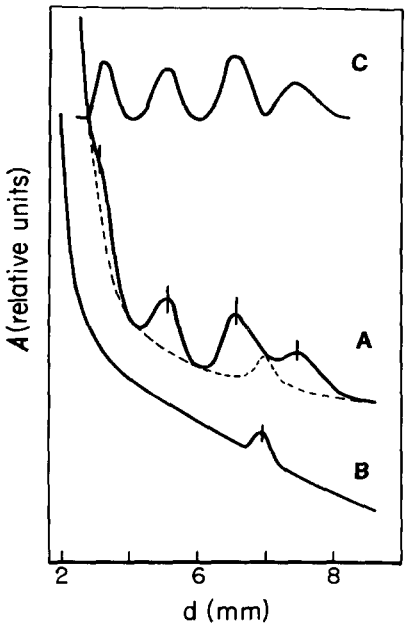

Fig. 1. Normal-incidence X-ray diffraction from mung bean outer mitochondrial membrane pellet. Curve A: solid line, hand-smoothed microdensitometer trace of X-ray diffraction pattern of specimen 1, Table I. Dashed line, background curve. (The monotonic portion of this curve was chosen such that the minima between rings 1 and 2, and 2 and 3 equal zero intensity. The peak near d = 7 mm in the background curve represents a reflection from the Al foil specimen support (see curve B), which was normalized for each diffraction trace such that the minimum between rings 3 and 4 equals zero intensity.) Curve B: hand-smoothed microdensitometer trace of the normal-incidence X-ray diffraction from a piece of Al foil like that used for specimen supports. Curve C: resulting diffracted intensity after subtraction of the dashed line from the solid line in (A). Note that the vertical displacement of curves A, B and C is arbitrary. Abbreviations: A, absorbance; d, distance along the film from the center of the zero-order maximum. Short vertical lines superimposed on the peaks of curves A and B indicate noise levels in these regions of the traces.

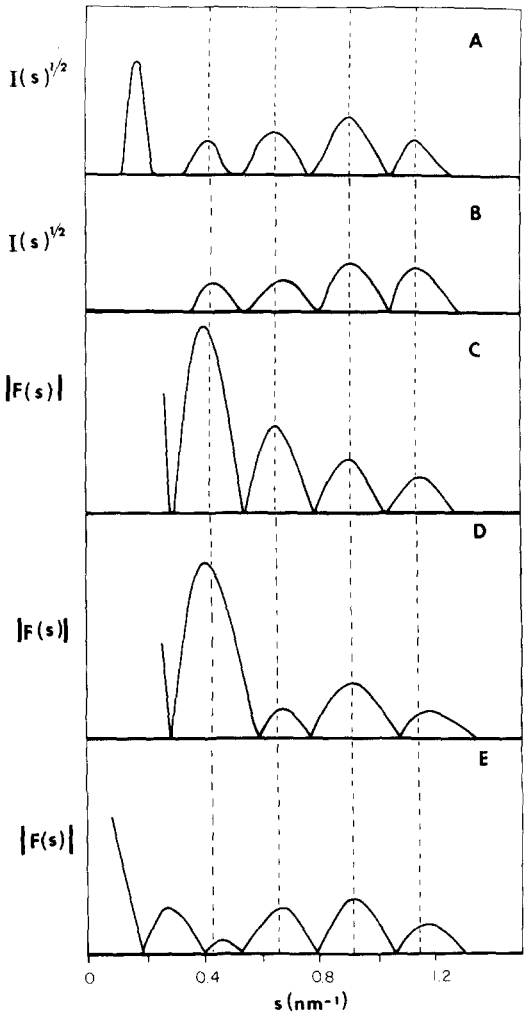

Fig. 2. Comparison of the observed normal-incidence X-ray diffraction from outer mitochondrial membranes with that expected for various model electron density profiles. Curves (A,B), square root of the radially integrated diffracted intensities from (A) Mung bean (specimen 1, Table I) and (B) potato (specimen 3, Table I) membrane specimens after 24–48 h at 75% relative humidity. Curves (C–E), moduli of the shape transforms calculated (see Appendix I) for centrosymmetric models described in the text: (C), circle of constant electron density contrast, diameter 4.0 nm; (D), ring of constant electron density contrast, inner diameter 1.0 nm, outer diameter 4.0 nm; (E), two infinitely thin rings of equal electron density contrast, diameters 4.3 and 2.4 nm. The vertical dashed lines are drawn from the centers of the four outermost maxima of curve A as an aid in aligning the peaks of subsequent curves.

note (***), Table I). In general, however, the intense diffuse background at small angle ($s < 0.3$ nm^{-1}) in these diffraction patterns made detection of maxima in this region very difficult.

The four or five normal-incidence diffraction maxima of curves 2A and 2B are evenly spaced and their positions approximately follow a n/D relation, for $D = 4.4$ nm and $n = 1, 2, 3 \ldots$ (see Table II). This could indicate the presence of lamellae with an interlayer spacing of 4.4 nm. However, several factors make it unlikely that this diffraction is actually due to a second lamellar phase in these membrane specimens. (a) The equatorial orientation of the related arcs in grazing-incidence diffraction patterns means that this second set of lamellae would have to be aligned perpendicular to the first, i.e., with bilayer surfaces parallel to the sedimentation direction. That a biological membrane structure would so align itself during centrifugation or during slow dehydration following centrifugation is very unlikely – or at least unprecedented. (b) Also, there is no systematic shift of the normal-incidence diffraction maxima to wider angle during slow dehydration of the membrane specimens. Such a decrease in interlayer spacing is expected during dehydration of lipid lamellae and is in fact observed with the meridional grazing-incidence diffraction from these same membranes.

The remaining explanation for the series of rings seen in normal-incidence diffraction patterns from the outer mitochondrial membrane specimens is that they arise from structure in the plane of the membranes in the (single) multilayer phase. This second interpretation is consistent with electron microscopic observations of prominent subunits in the plane of these membranes [5,6] and is used as the basis for the discussion that follows.

While the diffraction maxima of Fig. 2A and 2B can be approximately indexed to at least one two-dimensional lattice (hexagonal unit cell, lattice constant = 7.3 nm, see Table II), the Bragg reflections expected from such a lattice in the same region of reciprocal space total 19. The absence of about three-fourths of the maxima expected in this case, along with the obvious evenness in the separation between adjacent peaks in the observed diffraction patterns, argue against the maxima representing crystalline reflections from ordered arrays of membrane subunits (see discussion in Ref. 19). The

TABLE II

COMPARISON OF POSITIONS OF OBSERVED NORMAL-INCIDENCE DIFFRACTION MAXIMA WITH THOSE EXPECTED FOR SOME SIMPLE MODEL STRUCTURES

Symbols: D, lamellar repeat distance; a, unit cell dimension of lattice; R, radius of circle; n, order of lamellar reflections or of sequential maxima in shape transform of circle; h, k, Miller indices of crystalline reflections

Observed maxima		Predicted maxima					
Specimen 1 s (nm^{-1})	Specimen 3 s (nm^{-1})	Lamellae (D = 4.4 nm)		Hexagonal lattice (a = 7.3 nm)		Circle (R = 2.0 nm)	
		n	s (nm^{-1})	h, k	s (nm^{-1})	n	s (nm^{-1})
0.17	–	1	0.23	1, 0	0.16		
0.43	0.43	2	0.45	2, 1	0.42	1	0.41
0.65	0.67	3	0.68	4, 0	0.63	2	0.65
0.91	0.90	4	0.91	6, 0	0.95	3	0.91
1.14	1.13	5	1.14	4, 4		4	1.15
				5, 3	1.10–1.11		
				7, 0			

alternate intepretation is that the observed diffraction maxima arise from the shape transform, $F(s)$, of identical subunits present in essentially random array in the plane of the membrane. (This conclusion is in agreement with the reported random arrangement of outer membrane subunits seen in electron micrographs of negatively stained plant mitochondria [5,6].)

It was found that the positions of the four wider-angle maxima in the normal-incidence X-ray diffraction patterns coincide with the first four side maxima in the moduli of the shape transforms of a 4.3-nm diameter sphere or of a 4.0-nm diameter disk. (See Table II and Fig. 2C. Expressions used in the calculation of shape transforms presented in this section are summarized in Appendix I). However, for these simple model electron density profiles, the amplitudes of the side maxima decrease continuously with scattering angle, which is not the case with the observed maxima intensities. Hollow cylinder models could be found for which maxima in $|F(s)|$ approximately match the positions and intensities of the three observed wider-angle peaks (Fig. 2, curve D), but these models could not account for the low amplitude of the reflection at 0.43 nm^{-1} in the observed diffraction patterns.

Model for in-plane membrane structure based on Patterson function analysis

As previously reported [8], the radial Patterson function of the normal-incidence X-ray diffraction data from these membranes, equal to the Fourier transform of $I(s)$ into real space, contains prominent maxima at 1.1, 1.9, 3.4 and 4.3 nm. Peaks in this function, which is the rotationally averaged self-convolution product or autocorrelation function of the planar projection of the membrane electron density, represent often-realized distances between scattering centers on this projection. It was found that the simplest centrosymmetric model consistent with this radial autocorrelation function is composed of two concentric rings of equal electron density contrast in the membrane plane, with diameters given (approximately) by the positions of the largest and third-largest autocorrelation vectors (i.e., 4.3 and 1.9 nm). Fig. 2E illustrates that $|F(s)|$ for such a concentric ring model would be generally consistent with the observed diffraction at $s > 0.3$ nm^{-1}. The particular model used to calculate the shape transform of Fig. 2E also predicts an additional maximum in the transform at smaller angle, 0.29 nm^{-1}. As noted above, peaks were in fact observed below 0.3 nm^{-1} in normal-incidence diffraction

patterns of two of the outer mitochondrial membrane specimens after gradual dehydration. It may be that, in the other cases, the steepness of the background intensity in this region prevented detection of similar maxima. However, when considering the X-ray scattering in this small-angle region, one must also take into account the close-packing of the subunits seen in electron micrographs of these membranes [5,6]. This raises the possibility that the diffraction in this region contains contributions from interparticle vectors and that the apparent variability in the maxima at $s < 0.3$ nm^{-1} may be related to differences in packing of the membrane subunits within these specimens. On the other hand the constancy in the positions and relative intensities of the maxima observed at $s > 0.3$ nm^{-1} suggests that such interference terms are less significant at wider angle.

Calculation of the planar projection of the membrane subunit

By applying the phases predicted by the centrosymmetric model derived from Patterson function analysis (+–+–) to the four outermost maxima in the continuous scattering curve of Fig. 2A, a limited Fourier synthesis of the X-ray diffraction data can be performed (see Appendix I). The corresponding radial electron density, $\rho(r)$, is presented in Fig. 3. As might be expected from the above model analysis, this $\rho(r)$ contains two prominent maxima at $r = 1.2$ and 2.3 nm. Model calculations indicate that the damped oscillations in $\rho(r)$ at large values of r and the small peak at $r = 0.3$ nm can be attributed to wide-angle truncation of the diffraction data. Similarly, the steep drop in electron density below background which occurs between the two strong maxima (at $r = 1.75$ nm) in Fig. 3 can be accounted for, at least in part, by the absence of small-angle components from the Fourier synthesis. As noted above, the normal-incidence scattering data from the membrane specimens is unreliable below 0.3 nm^{-1}, because of the intense zero-order background and the possibility of interparticle scattering contributions at small angle. In principle one can attempt to refine $\rho(r)$ by constructing hybrid shape transforms, composed of $F(s)$ for appropriate models at small angle and $I^{1/2}(s)$, phased as above, at larger angle. While this approach has been used in the analysis of X-ray diffraction from various biological specimens (e.g. bacterial pili [20] and outer envelopes [19]), we find that the results depend heavily on the normalization of the two halves of such curves, which, as Burge and Draper [21] have noted, is somewhat arbitrary.

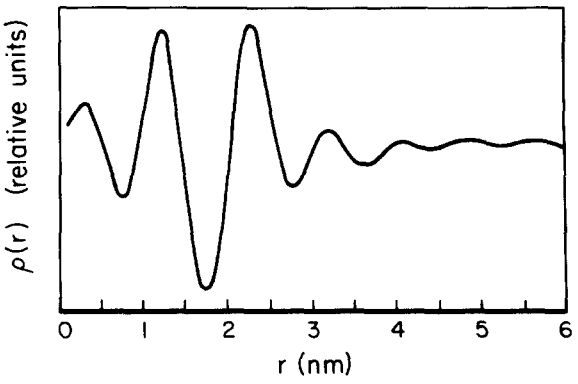

Fig. 3. Radial electron density profile calculated using the X-ray diffraction data of Fig. 2A, with phases assigned according to the two-ring model described in the text. The curve corresponds to a Fourier synthesis involving diffraction data within the limits $0.3 \leq s \leq 1.3$ nm^{-1}.

Possible interpretation of the radial electron density profile

Because the membranes in the normal-incidence diffraction experiments were unoriented with respect to rotation about the X-ray beam axis, the diffracted intensity can only provide information about the rotational average of the lateral structure of the membranes. The simple models discussed in the above analysis (circles, concentric rings) would represent approximations to the actual planar projections of the putative subunits only if the projections themselves have radial symmetry. Assuming this were the case, and further assuming that the concentric ring model were correct, the two rings could represent concentric cylindrical shells aligned normal to the membrane plane. The electron density profile of Fig. 3 would then predict an outer subunit diameter in the membrane plane of 5.0 nm and an inner, low-electron-density core of 1.8–2.0 nm. The outer diameter would be consistent with the closest center-to-center spacing of the pore-like subunits seen in electron micrographs of these membranes [5,6].

The low electron density at the center of the profile could, in turn, represent central pits (aqueous channels?) in the subunits. The inferred inner diameter would be consistent with the lower limit of the diameters of the sites of negative-stain accumulation (2–3 nm [5,6]) seen along the surface of these membranes in electron micrographs, but smaller than a recent estimate of the effective pore size of voltage-dependent anion-specific channel-forming activity (4 nm [10]), the channel-forming protein detergent complex isolated from outer mitochondrial membrane fractions.

Appendix I

The mathematical expressions used to calculate the shape transforms of Fig. 2 and the radial electron density profile of Fig. 3 are summarized for convenience in this section. (For detailed discussion of the principles and assumptions behind their derivation, see e.g. Ref. 22.)

The diffracted intensity, $I(s)$, from a single object (or from a dilute, random, monodisperse collection of spherically symmetric objects) is proportional to the square of the modulus of $F(s)$, the structure factor or shape transform of the object – i.e. the Fourier transform of the electron density distribution of the object, $\rho(r)$, into reciprocal space.

In two dimensions, the Fourier transform of a radially symmetric electron density distribution, $\rho(r)$, is given by

$$F(s) = 2\pi \int_0^\infty \rho(r)\, J_0(2\pi rs)\, r\, \mathrm{d}r \qquad (1)$$

where J_n is a cylindrical Bessel function of order n.

The expression for $F(s)$ is simplified when the electron density is that of a circle of diameter D with constant electron density contrast $\Delta\rho$:

$$\rho(r) = \begin{cases} \Delta\rho & r \leqslant D/2 \\ 0 & r > D/2 \end{cases}$$

$$F(s) = \Delta\rho\, D J_1(\pi D s)/2s$$

Just as a circle can represent the projection of a right-circular cylinder in the membrane plane, the projection of a hollow cylinder can be expressed as the difference of the electron densities of two concentric circles, $\rho_1(r)$ and $\rho_2(r)$, of equal electron density contrast and diameters $D_1 < D_2$:

$$\rho(r) = \rho_2(r) - \rho_1(r) = \begin{cases} \Delta\rho & D_1/2 \leqslant r \leqslant D_2/2 \\ 0 & D_1/2 \geqslant r \geqslant D_2/2 \end{cases}$$

$$F(s) = \frac{\Delta\rho}{2s}\left(D_2 J_1(\pi D_2 s) - D_1 J_1(\pi D_1 s)\right)$$

In the case of n infinitely thin rings of electron density contrast $\Delta\rho$ at radii $D_i/2$ ($i = 1$ to n), the radial electron density can be expressed in terms of the sum of Kronecker delta functions:

$$\rho(r) = \Delta\rho \sum_{i=1}^{n} \delta(D_i/2)$$

and the corresponding shape transform, by Eqn. 1, is:

$$F(s) = 2\pi \int_0^\infty \Delta\rho \left[\sum_{i=1}^{n} \delta(D_i/2)\right] J_0(2\pi rs)\, r\, \mathrm{d}r$$

$$= \pi\, \Delta\rho \sum_{i=1}^{n} D_i J_0(\pi D_i s)$$

The continuous radial electron densities of Fig. 2 were calculated by the inverse of the Fourier transform of Eqn. 1:

$$\rho(r) = 2\pi \int_0^\infty F(s)\, J_0(2\pi sr)\, s\, \mathrm{d}s \qquad (2)$$

$F(s)$ is defined over each interval j in s, corresponding to each of the m maxima in $I(s)$, by:

$$F(s) = \sum_{j=1}^{m} \{\pm\}_j I_j^{1/2}(s) \qquad (3)$$

where the phases (+ or –) can be derived from centrosymmetric models (see text). Numerical computation of $\rho(r)$ according to expressions 2 and 3 were carried out, for $r = 0.1$ to 10.0 nm, as the sum

$$\rho(r) = 2\pi \sum_{k=k_1}^{k_2} F(k\,\Delta s)\, J_0(2\pi rk\,\Delta s)\, k(\Delta s)^2$$

where Δs was equal to $6.5 \cdot 10^{-3}$ nm^{-1} and $k_1\Delta s$ and $k_2\Delta s$ represented the lower and upper truncation limits to the diffraction data in each case (see text).

Acknowledgements

I thank Dr. Donald F. Parsons for his advice and encouragement in the course of this research, Dr. George W. Brady for critically reviewing this manuscript and Dr. W.R. Moyer and his staff for assistance in the use of the computer facilities of the Division of Laboratories and Research.

References

1 Werkheiser, W.C. and Bartely, W. (1957) Biochem. J. 66, 79–91
2 Pfaff, E., Klingenberg, M., Ritt, E. and Vogell, W. (1968) Eur. J. Biochem. 5, 222–232
3 Wojtczak, L. and Zaluska, H. (1969) Biochim. Biophys. Acta 193, 64–72
4 Douce, R., Mannella, C.A. and Bonner, W.D., Jr. (1973) Biochim. Biophys. Acta 292, 105–116
5 Parsons, D.F., Bonner, W.D., Jr. and Verboon, J.G. (1965) Can. J. Bot. 43, 647–655
6 Parsons, D.F., Williams, G.R. and Chance, B. (1966) Ann. N.Y. Acad. Sci. 137, 643–666
7 Mannella, C.A. and Bonner, W.D., Jr. (1975) Biochim. Biophys. Acta 413, 213–225
8 Mannella, C.A. and Bonner, W.D., Jr. (1975) Biochim. Biophys. Acta 413, 226–233
9 Colombini, M. (1979) Nature 279, 643–645
10 Colombini, M. (1979) Ann. N.Y. Acad. Sci. 341, 552–562
11 Zalman, L.S., Nikaido, H. and Kagawa, Y. (1980) J. Biol. Chem. 255, 1771–1774
12 Mannella, C.A. and Ratkowski, A.J. (1979) J. Cell Biol. 83, 270a
13 Shipley, G.G. (1973) in Biological Membranes (Chapman, D. and Wallach, D.F., eds.), Vol. 2, pp. 1–89, Academic Press, New York
14 Thompson, J.E., Coleman, R. and Finean, J.B. (1968) Biochim. Biophys. Acta 150, 405–415
15 Wattiaux-de Coninck, S., Dubois, F. and Wattiaux, R. (1977) Biochim. Biophys. Acta 471, 421–435
16 Blaurock, A.E. and Wilkins, M.H.F. (1969) Nature 223, 906–909
17 Henderson, R. (1975) J. Mol. Biol. 93, 123–138
18 Lesslauer, W. (1980) Biochim. Biophys. Acta 600, 108–116
19 Ueki, T., Mitsui, T. and Nikaido, H. (1979) J. Biochem. 85, 173–182
20 Folkhard, W., Leonard, K.R., Malsey, S., Marvin, D.A., Dubochet, J., Engel, A., Achtman, M. and Helmuth, R. (1979) J. Mol. Biol. 130, 145–160
21 Burge, R.E. and Draper, J.C. (1971) J. Mol. Biol. 56, 21–34
22 Hosemann, R. and Bagchi, S.N. (1962) Direct Analysis of Diffraction by Matter, North-Holland, Amsterdam